EFFECT OF RADIAL POWER PROFILE ON ENDPLATE INTEGRITY

M. TAYAL*, B. WONG*, Y. SHUDOH**

* Atomic Energy of Canada Limited, Mississauga, Canada
** Electric Power Development Company Limited, Tokyo, Japan

ABSTRACT

Differential enrichment of uranium and/or radial gradients of neutron flux generally result in a non-uniform power profile along the radius of a CANDU® fuel bundle. This bends the endplates. This paper describes a methodology to assess the resulting elastic/plastic stresses/strains in the endplate. A failure criterion is proposed, along with an illustrative example.

INTRODUCTION

In a CANDU* fuel bundle, fuel elements in the various rings (see Figure 1a) operate at different powers because of radial gradients of neutron flux. This leads to differential thermal axial expansions of the fuel elements in the various rings. The differential element lengths bend the endplate, see Figure 1b. This generates stresses and strains in the endplate.

In natural-uranium CANDU fuel bundles, the degree of endplate bending is small enough that no current CANDU endplate has ever failed from the above mechanism. In some of the advanced fuel cycles that are now being proposed for the CANDU reactors, different levels of uranium enrichment are being suggested for the various rings. One example is the Advanced Large Scale (ALS) CANDU reactor (1). This leads to steeper gradients of element powers, see Figure 2, and a greater degree of endplate bending.

The objective of this study was to confirm that the endplates will not fail due to the higher bending strains expected in the ALS CANDU reactor.

The text first provides some technical background pertinent to the specific conditions assessed in this study. Then a failure criterion is established for endplate strain as a function of neutron dose. This is followed by assessments of length-differentials and of endplate stresses/strains.

---

* CANDU®: Canada Deuterium Uranium is a registered trademark of Atomic Energy of Canada Limited

Presented at the Fourth International Conference on CANDU Fuel, Pembroke, Canada, 1994 October 1-4. Sponsored by CNS, COG, IAEA.

BACKGROUND

The scope of this study was limited to assessments of endplate stresses and strains due to length differentials among the fuel elements of a slightly-enriched uranium (SEU) CANFLEX (2) fuel bundle, see Figure 1a. The bundle was considered to experience the power-ramps expected in the ALS CANDU reactor (1). The reactor contains 632 fuel channels and its gross electrical output is 1235 MWe. The core-average discharge burnup is 21 GW.d/tU. To achieve this, the fuel elements contain slightly enriched uranium in the outer two rings. Depleted uranium is used in the inner two rings. The bundle also contains some burnable poison (1).

Reactor physics simulations provided the power histories and the power ramps in the different rings. The maximum bundle-average burnup is about 600 MW.h/kgU while the maximum element burnup is about 800 MW.h/kgU. Generally, the power and the size of the power-ramp decrease with burnup.

FAILURE CRITERION

The ductility of Zircaloy decreases with fluence. Figure 3 shows a compilation of tensile test data of Yamashita et. al (3) and of Hardy (4).

Element-length-differentials impose secondary (rather than primary) stresses and strains in the endplate. For this reason, we used only that experimental data which was obtained from secondary tensile strains. Data based on primary stresses, such as data collected using burst tests, were excluded. As well, some of the reported data were excluded because they were directed primarily at determining the influence of various levels of defects on the ductility of irradiated Zircaloy.

The data in Figure 3 show considerable scatter. Nevertheless, there is a clear trend towards decreasing ductility with increasing fluence.

We fitted the following design-centre curve to the above data:

$$\frac{\varepsilon}{\varepsilon_o} = c_1 + (1 - c_1) e^{-\sqrt{\frac{\Phi}{c_2}}}$$

where ε = strain-to-failure (%) at fluence ϕ; ε_o = strain-to-failure (%) at zero fluence; ϕ = fast fluence (n/cm^2); $c_1 = 0.13$; $c_2 = 4.78 \times 10^{20}$; and e = exponential.

We used this curve as our failure criterion. Thus, we compared the above ductility to the maximum incremental strains in the endplate due to the power-ramps at various burnups. The incremental endplate strains, in turn, were calculated using the incremental differential lengths of fuel elements during the power-ramps. This is described in the next section.

LENGTH DIFFERENTIAL

The ELESTRES code (5) was used to calculate the length differentials among the elements at the different endplate rings. Thus, our assessment included on-power effects including: thermal expansion, densification, fission product swelling, collapsible cladding, pellet cracking, and elastic/plastic/creep deformation of the pellet.

The differential length is the highest, about 2 mm, when the fuel is first brought to full power. With increasing burnup, the power ramps become smaller, see Figure 4a. The same behaviour applies to the incremental differential lengths, see Figure 4b. At the exit burnup, the incremental differential length is negligible.

METHOD FOR CALCULATING ENDPLATE DEFORMATION

The finite element code MARC (6) was used to calculate the endplate stresses and strains.

The following major features of the MARC code were used: elastic-plastic analyses; large displacements; updated Lagrangian formulation; and thick-shell finite elements. Brief descriptions of these are given below.

Elastic-plastic analyses enabled us to alter the local strength of the endplate as a function of the local stress. The elastic-plastic calculations used an incremental approach. This means that the external displacements/loads were increased gradually, in relatively small increments, from their initial values to their final values. At each increment, the additional plastic flow was calculated based on the stresses reached during the previous increment. We used the Von Mises formulation for the yield surface, and the Prandtl-Ruess flow rule. This approach permits one to account for the dynamic changes in the local stress distribution caused by plastic flow.

The 'large displacement' formulation was used to calculate the local strains from the local displacements. This formulation includes several second order terms, for example, the gradients of local rotations, that are usually ignored in most analyses. But we included them here because the expected deflection of the endplate is similar to its thickness and hence is considered relatively 'large' in this context.

In formulating the stiffness matrices, the 'updated Lagrangian' technique was used. In this technique, the geometric component of the stiffness matrix is updated at each increment, based on the geometry calculated in the previous increment. This feature was considered desirable in view of the relatively large displacements of the endplate.

'Thick-shell' finite elements were used rather than the more common 'beam' elements. This enabled us to subdivide the endplate rings and ribs into a number of segments across their widths. This gave a more detailed numerical representation of the endplate, consequently higher accuracy.

Figure 5 shows the finite element mesh for the endplate. It uses triangular elements arranged in a hexagonal pattern. Previous experience suggests that this combination generally gives the highest accuracy (5,7).

The mesh is fine in areas of high stresses and of high gradients of stresses. When there are several similar areas of high concentrations of stresses, only one representative segment has a fine mesh and the remaining have relatively coarse meshes. Coarse mesh is also used in areas of relatively low stresses. Thus six regions are represented by fine meshes, and are labelled A to F in Figure 5. With these features we could obtain the detailed local stresses in the critical regions, along with the overall responses of the remaining regions, while minimizing the computing costs.

The resulting mesh contains 1021 nodes and 1465 finite elements in the endplate. Each finite element was further subdivided into seven layers through its thickness. This enabled us to account for partial plasticity through the thickness of the endplate.

The interactions between the endplate and the fuel elements were simulated via springs. The appropriate spring constants were obtained by using the BEAM code (8). Thus, on-power pellet/sheath interaction was reflected in the assessment.

ENDPLATE BEHAVIOUR

Figure 6 shows a typical deformed shape of the endplate for a length differential of 2 mm. The dishing of the endplate is quite noticeable. The maximum strain occurs at the junction of the long radial rib and the intermediate ring. This reflects the combined influences of the following parameters: degree of local bending; local stress concentrations due to the junction of radial ribs and circumferential rings; and stress concentrations due to the junctions between fuel elements and endplates.

Figure 7 shows the evolution of endplate strain at different locations. Again, it is clear that the intermediate ring develops the highest strains, while the outer ring has negligible strains.

The endplate becomes plastic when the length differential reaches 0.35 mm. Our analysis accounted for plastic flow at higher length differentials.

For the highest length-differential, 2 mm, the maximum effective stress is 241 MPa and the maximum principal stress is 274 MPa. The maximum strain is 3.2%. This occurs when the fuel is first brought to power. At this time the ductility of Zircaloy is about 15%, hence a strain of about 3% poses no threat to endplate integrity.

Figure 4c shows the endplate strains for power ramps at different burnups. The corresponding failure limits are also shown. It is clear that the strains are well below the corresponding failure limits. Hence we expect the endplate to maintain its structural integrity under the above conditions.

SUMMARY AND CONCLUSIONS

Within a fuel bundle, steeper radial gradients of element power increase the axial bending of the endplate. We assessed the resulting endplate strains in a SEU/CANFLEX bundle experiencing the power-ramp of an Advanced Large Scale (ALS) CANDU reactor.

In the endplate, the intermediate ring generally contains the highest stresses/strains because the endplate bends the most at that location. The endplate stresses/strains peak near the fuel element that is closest to the junction of the intermediate ring and the long radial rib.

The stresses and strains in the endplate stay elastic for length-differentials less than 0.35 mm, and become plastic at higher length-differentials. When the fuel is first brought to power, the length-differential is about 2 mm. This gives a maximum effective stress of 241 MPa, and a maximum principal stress of 274 MPa. The maximum strain is 3.2%. At this time the ductility of Zircaloy is about 15%, hence strains of about 3% poses no threat to endplate integrity.

Irradiation reduces the ductility of Zircaloy. But irradiated fuel also experiences much smaller power-ramps, hence much smaller incremental strains. We examined the above effects for a range of burnups up to 800 MW.h/kgU. For all burnups in this range, the incremental strains are well below the corresponding ductilities. Hence the endplate is not at risk of failure from this mechanism.

ACKNOWLEDGEMENTS

The authors thank R. Mak, K. Hallgrimson, Mr. Y. Yoneda, Mr. S. Sato, M. Gacesa, D. Sears, T. Carter, S. Baset, A. Dastur, D. Bowslaugh, I.Oldaker, and J.Lau for their valuable inputs. Financial support from Electric Power Development Company Limited, Tokyo, Japan, is also gratefully acknowledged.

REFERENCES

1. A.R. Dastur, P.S.W. Chan, D. Bowslaugh, "The Use of Depleted Uranium for the Reduction of Void Reactivity in CANDU Reactors", 13th Annual Conference of the Canadian Nuclear Society, Saint John, New Brunswick, 1992 June 7-10.

2. A.D. Lane, R. Sollychin, B.A. Surette, B.M. Townes, H.S. Suk, B.W. Rhee, S.H. Jung, C.H. Chung, "The Status of the Program to Develop the CANFLEX Fuel Bundle", Third International Conference on CANDU Fuel, Canadian Nuclear Society, Chalk River, Canada, 1992 October 4-8.

3. K. Yamashita, T. Nomata, T. Yasuda, T. Aoki, "Effects of the Fast Neutron Irradiation on the Mechanical Properties of Recrystallized Zircaloy-2 Cladding", Post Irradiation Examination and Experience, Proceeding of a Specialists' Meeting held in Tokyo, Japan, 1984 November 26-30.

4. D.G. Hardy, "The Effect of Neutron Irradiation on the Mechanical Properties of Zirconium Alloy Fuel Cladding in Uniaxial and Biaxial Tests", Irradiation Effects on Structural Alloys for Nuclear Reactor Applications, American Society for Testing and Materials, ASTM STP 484, 1970, pp. 215-258.

5. M. Tayal, "Modelling CANDU Fuel Under Normal Operating Condition: ELESTRES Code Description", Atomic Energy of Canada Limited, Report AECL-9331, 1987.

6. "MARC General Purpose Finite Element Program: Volume A: User Information Manual", MARC Analysis Research Corporation, Palo Alto, California, U.S.A., 1988.

7. T. Udoguchi, H. Okamura, T. Kano, Y. Nozue, "An Error Analysis of Various Finite Element Patterns", Bulletin of the Japanese Society of Mechanical Engineers, 16, 102, 1973, pp. 1803-1813.

8. M. Tayal, B.J. Wong, J.H.K. Lau, A.M. Nicholson, "Assessing the Mechanical Performance of a Fuel Bundle: BEAM Code Description", Atomic Energy of Canada Limited, Report AECL-10643, 1992.

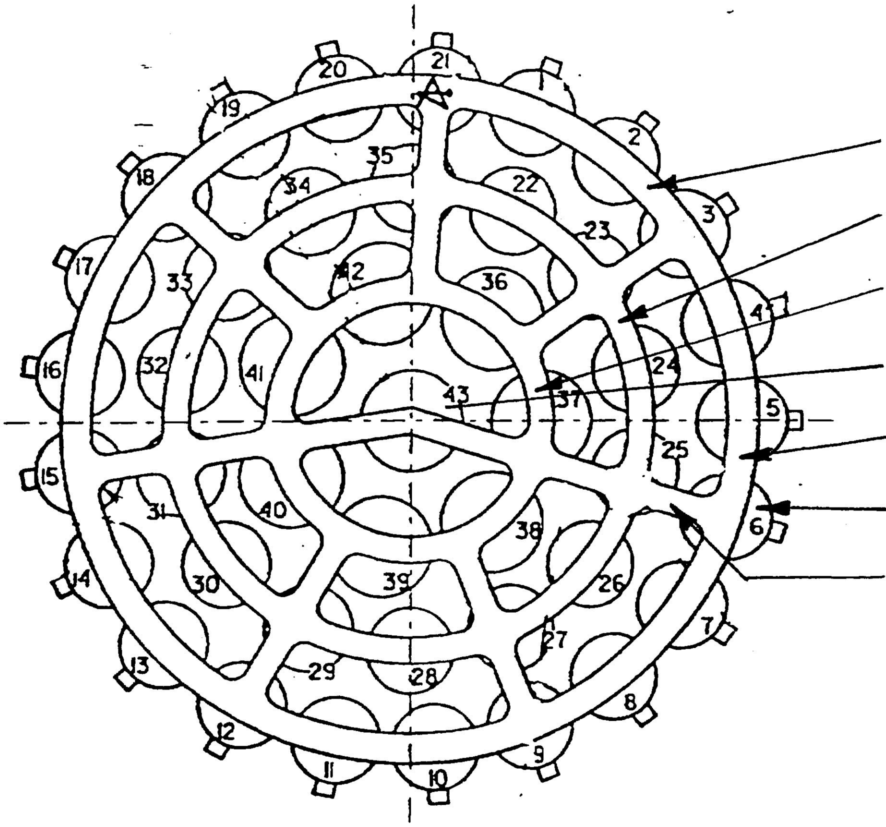

(a) Cross-Section

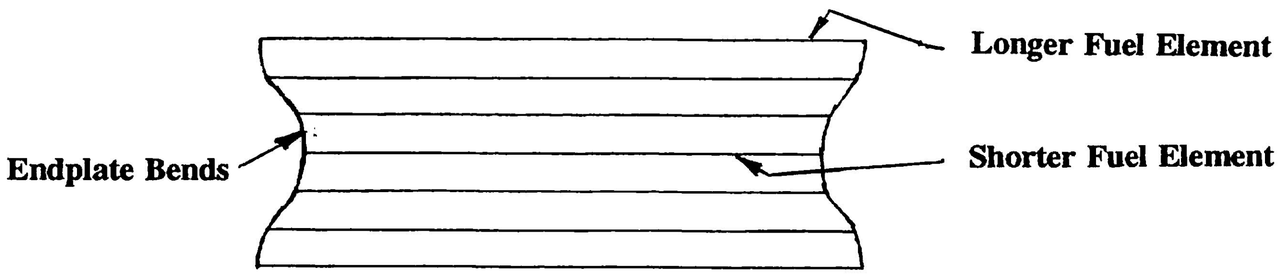

Note : For clarity, the endplate bending has been exaggerated

(b) Endplate Bending

Figure 1 : CANFLEX Bundle

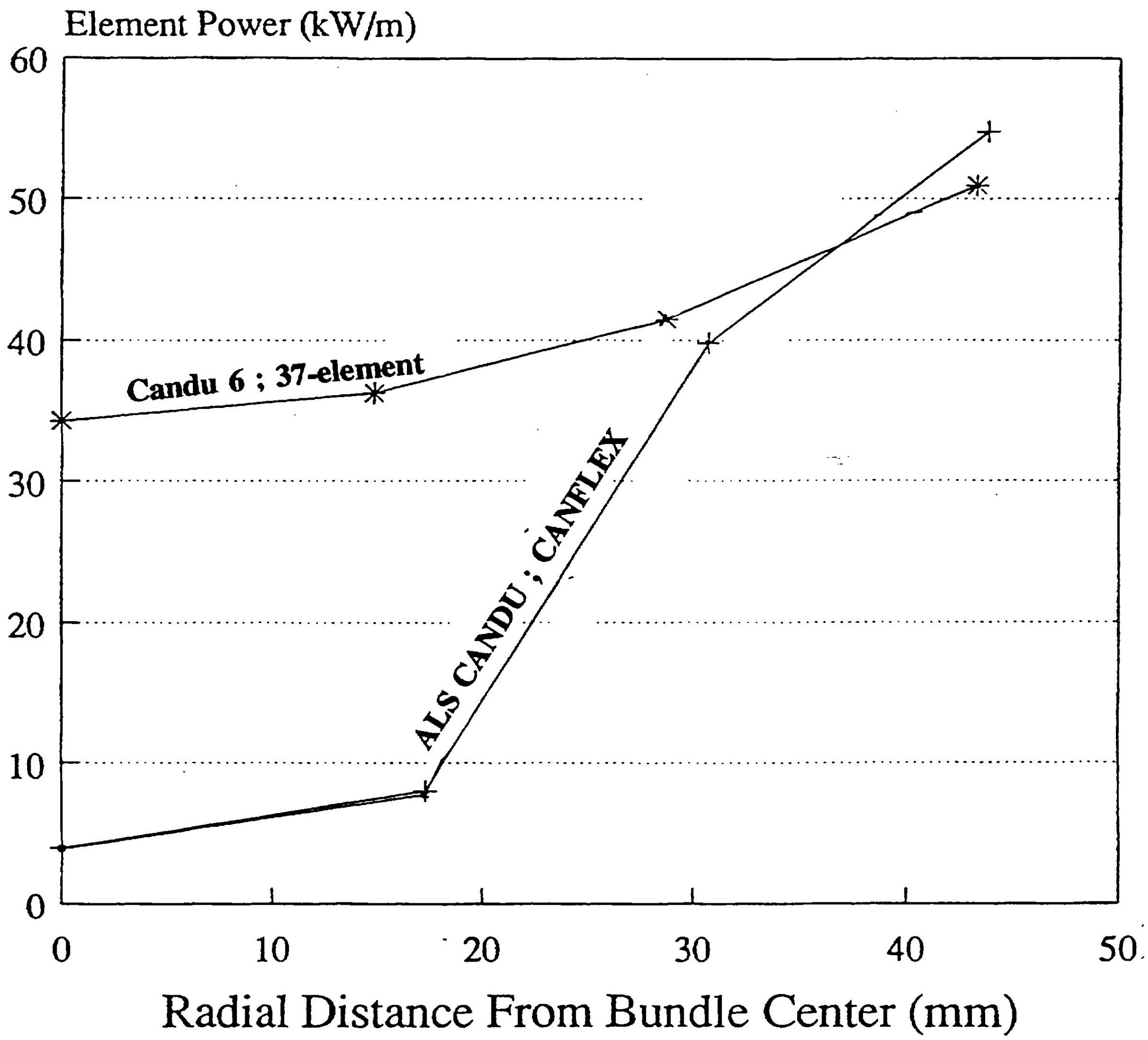

Figure 2 : Power Distribution Across Bundle Radius

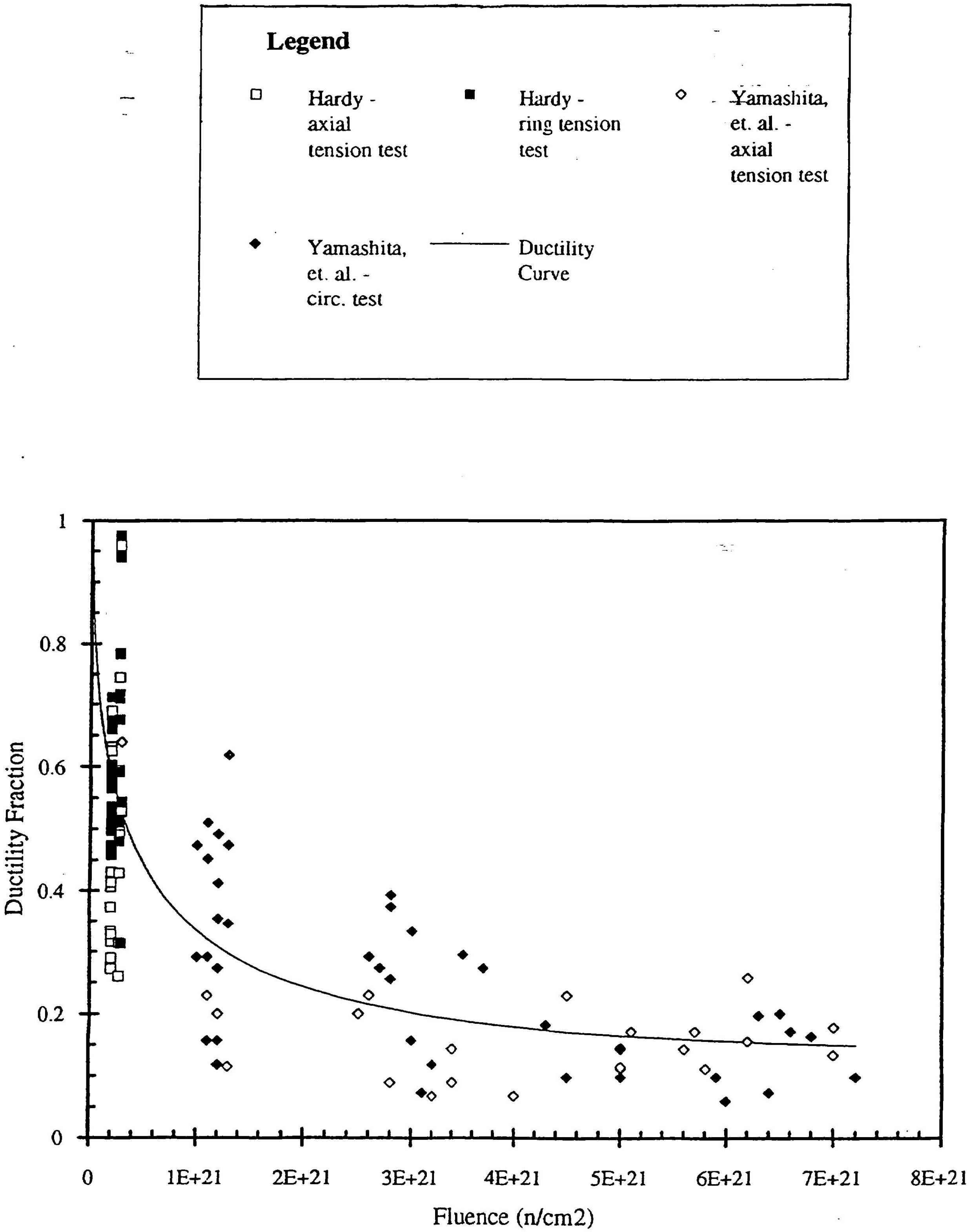

Figure 3 : Ductility Criterion

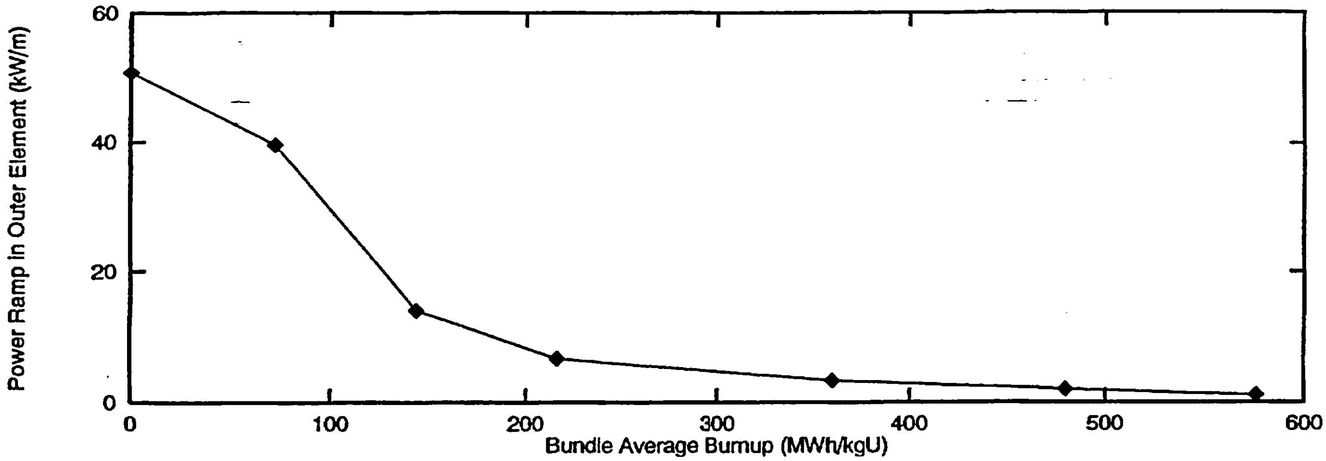

(a) Power Ramp

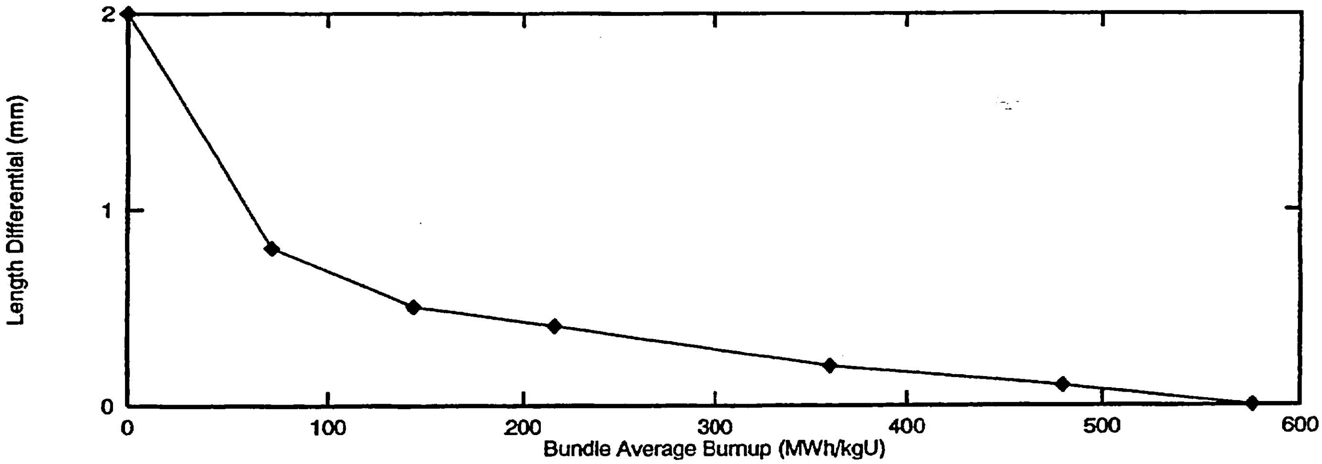

(b) Length Differential

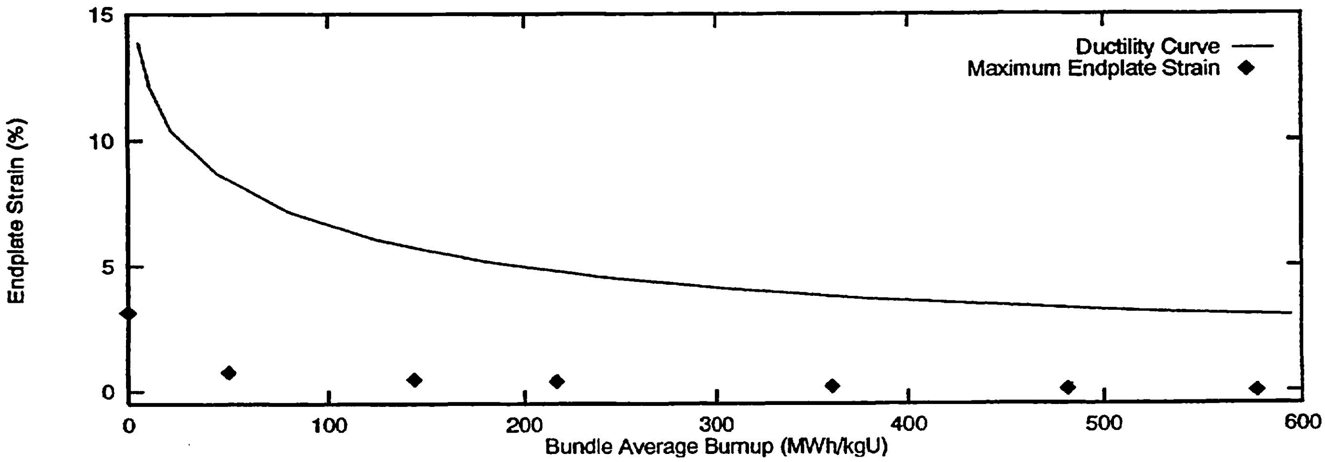

(b) Endplate Strain

Fig. 4 LENGTH DIFERENTIAL AND ENDPLATE STRAIN

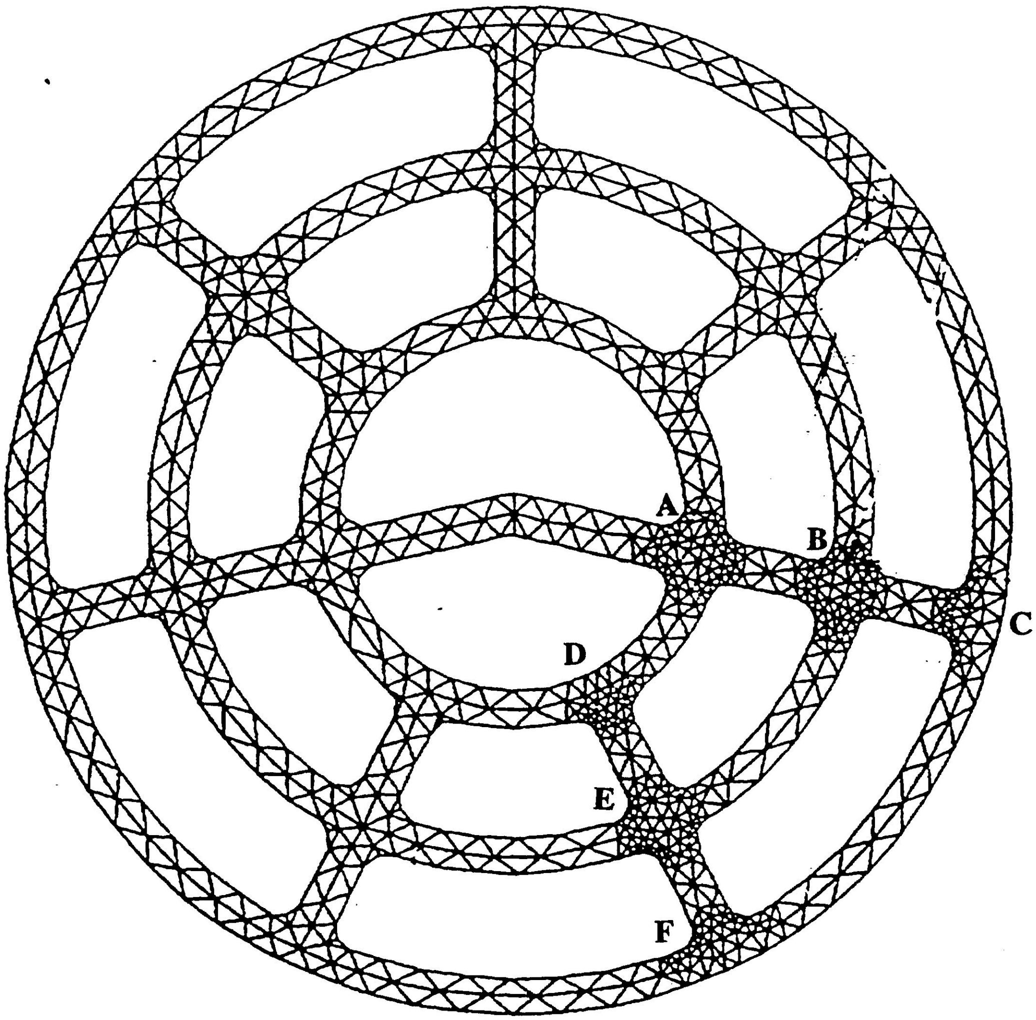

Figure 5 : Finite Element Mesh

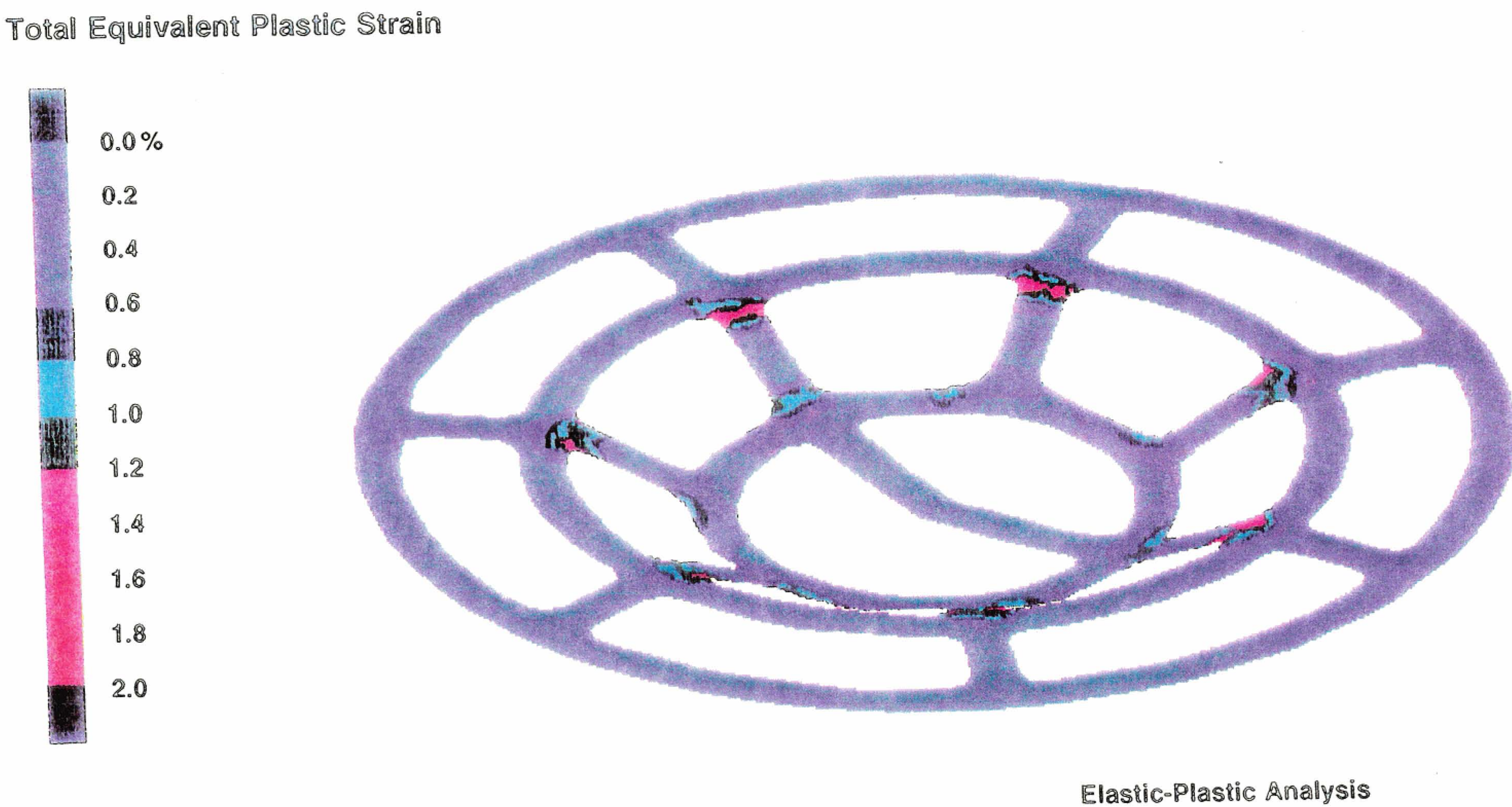

Note : For clarity, the displacements have been magnified by a factor of 5

Figure 6 : Deformed Shape of the Endplate

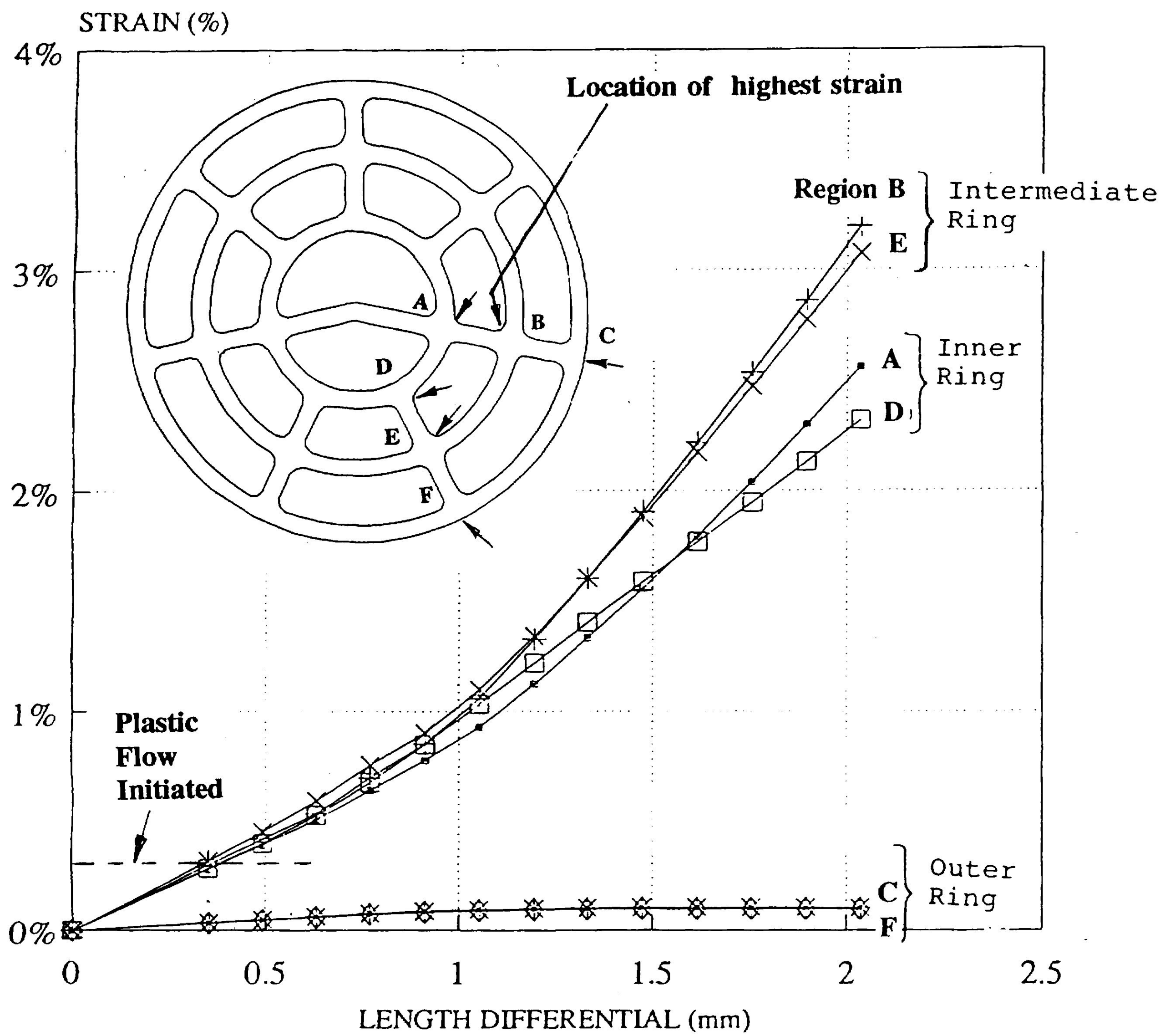

Note : The arrows indicate the spots within each region where the strain is the highest

Figure 7 : Evolution of Maximum Total Strains in the Endplate